Supporting Information

Closed-Loop Engineering of Chemically Anchored Lead-Carbon Composites via Thermodynamic-Kinetic Synergy for Ultra-Long-Life Lead-carbon Batteries

Jiecai Li [a], Yang Sun [a], Qilong Wang [a], Zhiqiang Liu [a], Yupeng Wu [a], Qinwen You [a], Xin Ding [a], Tangjun Wang [a], Chuanbo Wei [a], Guobing Wang [c], Nan Lin [a, b*] Haibo Lin [a**]

[a] State Key Laboratory of Inorganic Synthesis and Preparative Chemistry, Jilin University, Changchun 130012, Jilin, China

[b] National Demonstration Center for Experimental Chemistry Education, Jilin University, Changchun 130012, China

[c] Guangdong Yingyeda Electronics Co., Ltd, Guangzhou 510000, Guangdong, China

* Corresponding author.

** Corresponding author.

Email: nanlin@jlu.edu.cn (N. Lin), lhb910@jlu.edu.cn (H.B. Lin).

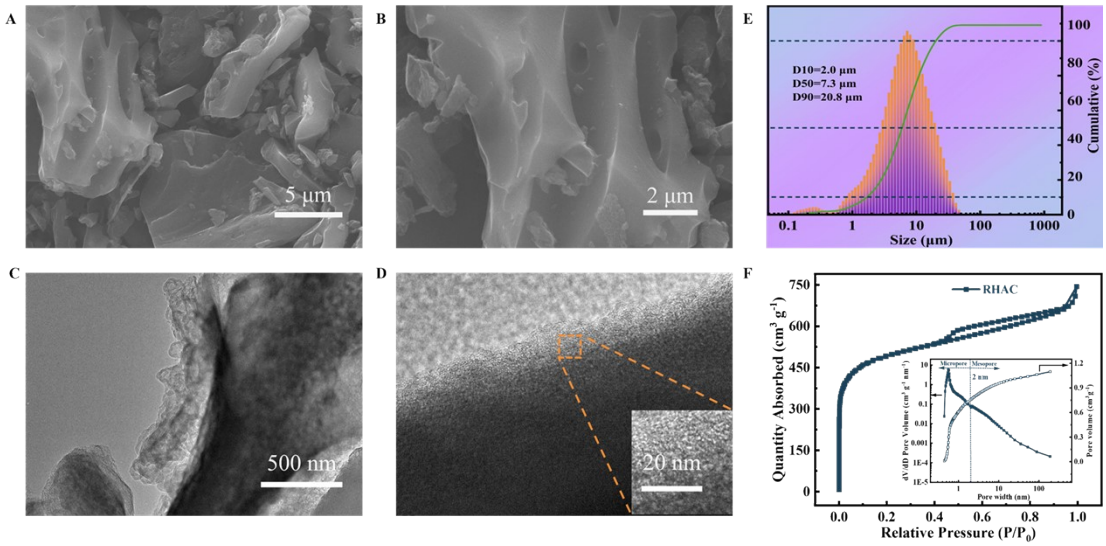

Fig. S1. RHAC of (A-B) SEM images, (C) TEM image, (D) HRTEM image, (E) particle size distribution curve; (F) N_2 adsorption-desorption isotherms curve, the inset shows the PSD curve obtained by the DFT method.

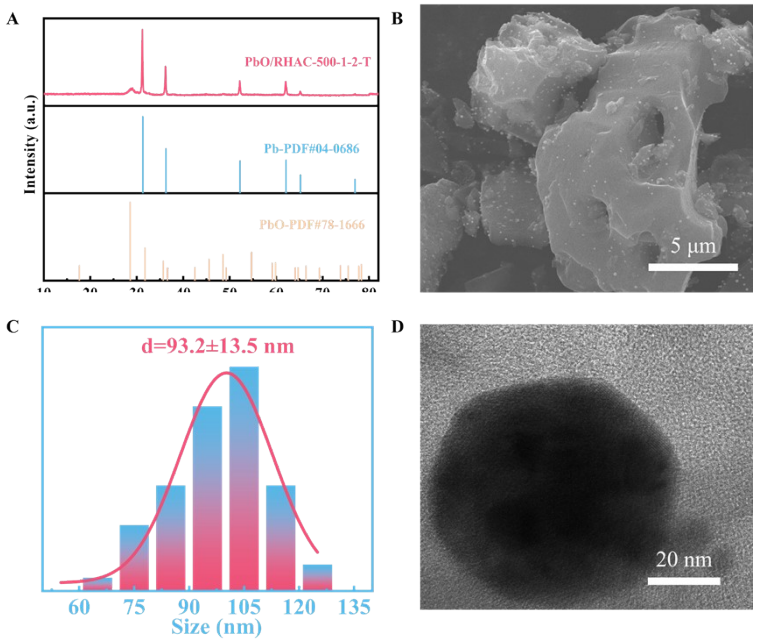

Fig. S2. (A) XRD pattern, (B) SEM image, (C) corresponding particle size distribution, and (D) TEM image of PbO/RHAC-500-1-2-T.

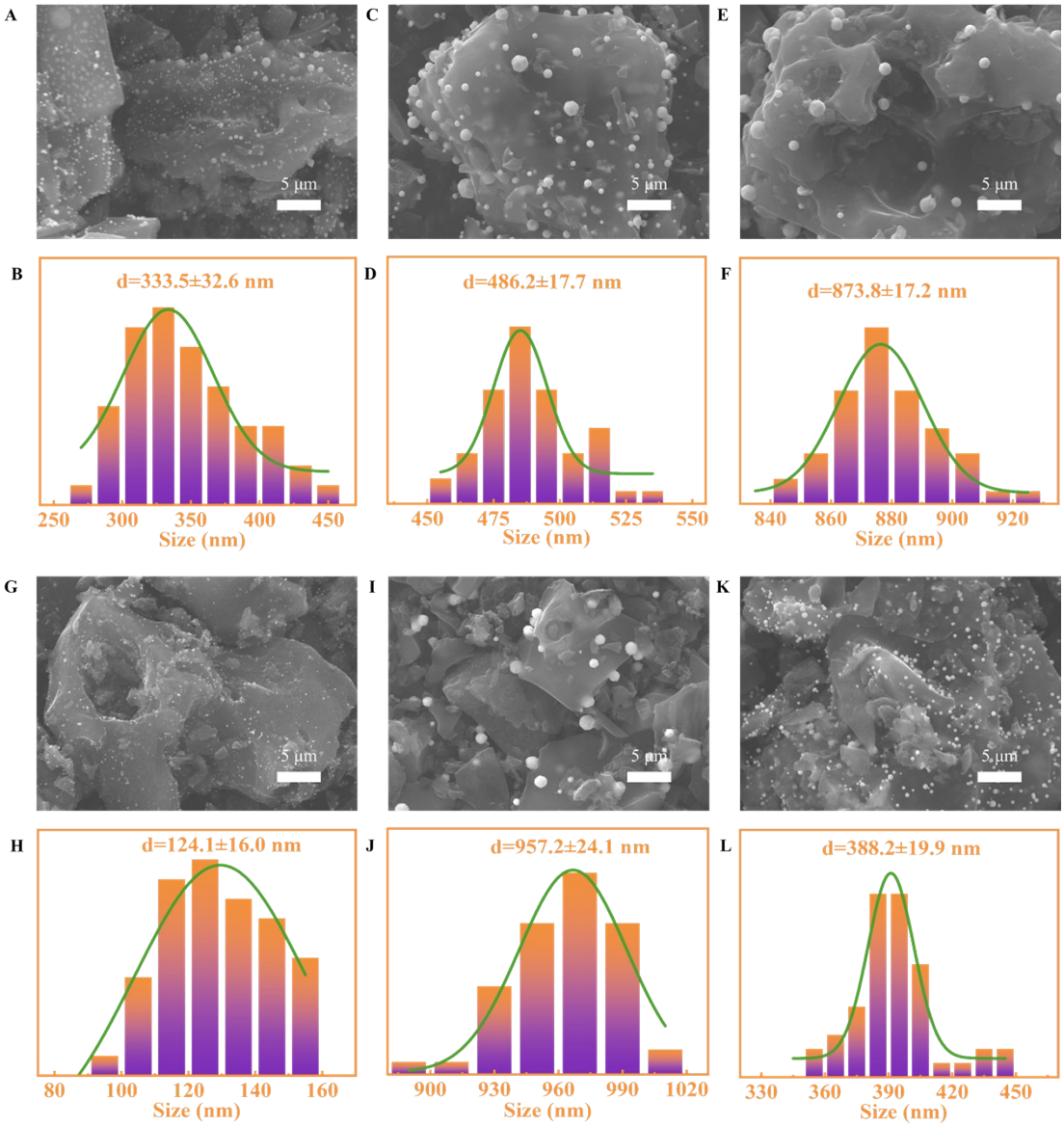

Fig. S3. SEM image and PbO particle size distribution histogram of (A, B) PbO/RHAC-500-1-2, (C, D) PbO/RHAC-500-2-2, (E, F) PbO/RHAC-500-3-2, (G, H) PbO/RHAC-400-2-2, (I, J) PbO/RHAC-550-2-2, and (K, L) PbO/RHAC-450-2-15. As the holding time increases, PbO particles undergo further sintering and coarsening. At 400 °C, the precursor decomposes incompletely, resulting in uniformly dispersed particles; at 550 °C, severe Ostwald ripening and agglomeration occur. Increasing the heating rate also leads to coarsening of the PbO samples.

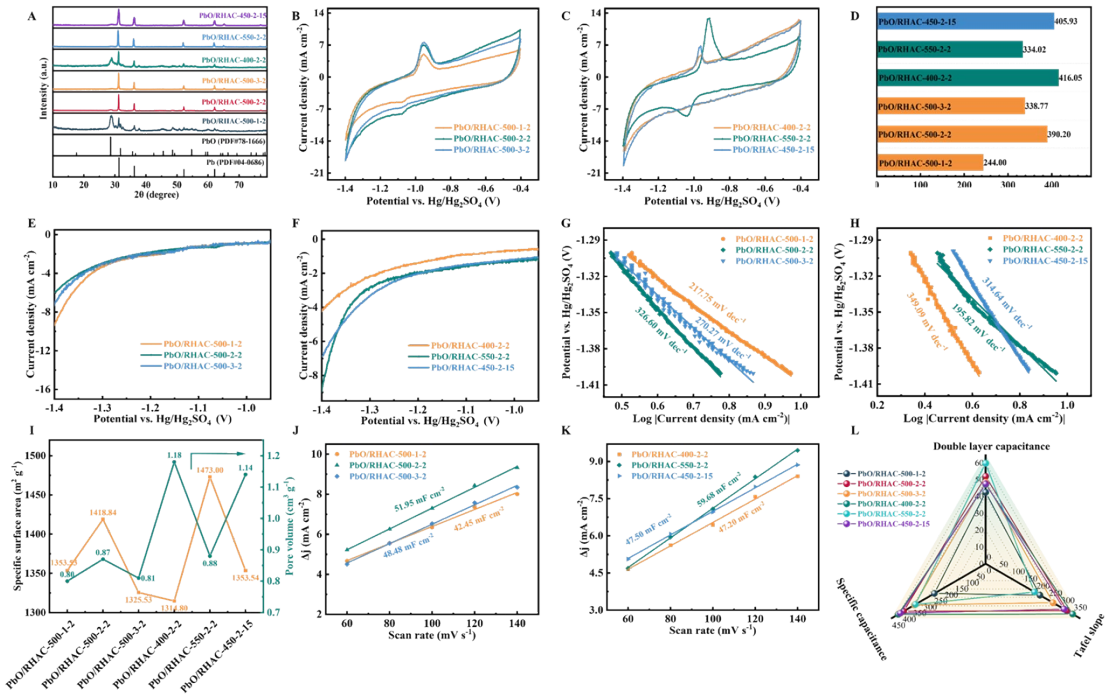

Fig. S4. (A) XRD pattern. (B-C) CV curves and (D) specific capacitance. (E-F) LSV curves and (G-H) Tafel plots. (I) Specific surface area and pore volume. (J-K) Double-layer capacitance. (L) Composite performance radar chart.

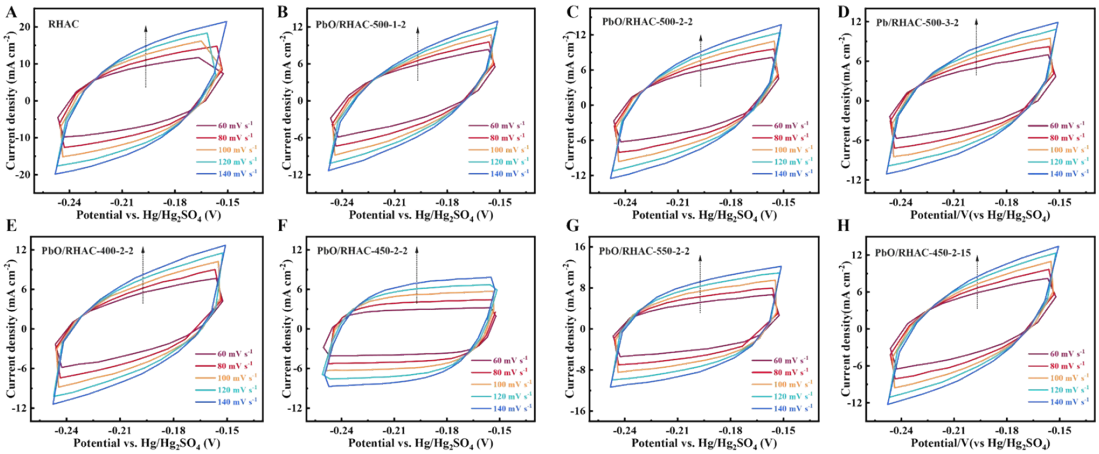

Fig. S5. CV curves of (A) RHAC, (B) PbO/RHAC-500-1-2, (C) PbO/RHAC-500-2-2, (D) PbO/RHAC-500-3-2, (E) PbO/RHAC-400-2-2, (F) PbO/RHAC-450-2-2, (G) PbO/RHAC-550-2-2, and (H) PbO/RHAC-450-2-15 at different scan rates.

Fig. S6. Photographs of the positive electrode (left) and negative electrode (right) after cycling: (A) Blank battery, (B) RHAC battery, (C) PbO/RHAC battery.

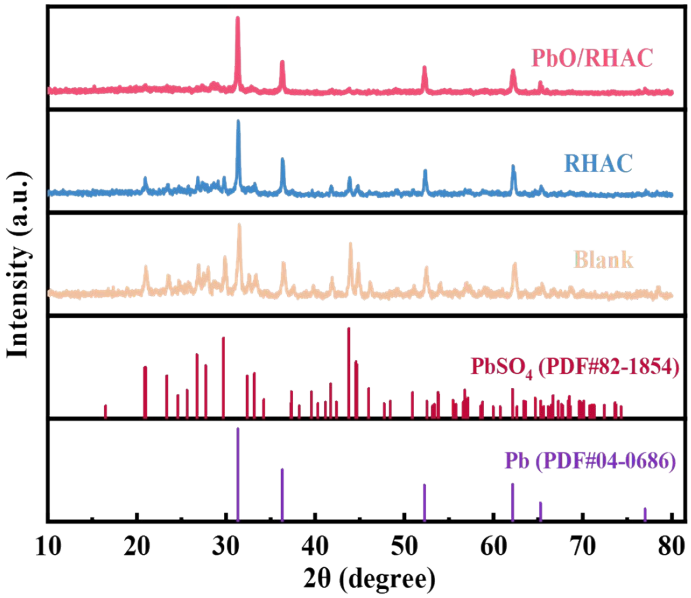

Fig. S7. XRD pattern of NAM after cycling.

Table S1. Process parameters for large-scale preparation of PbO/RHAC.

Number	Operating unit	Control parameter name	Control range
1	Complexation precipitation reaction	Temperature range	< 40 °C
		Impregnation pH	5 – 7
		Complexation precipitation pH	2 – 5
2	Solid liquid separation and washing	Temperature range	20 – 40 °C
		pH	5 – 7
		Pressure range	1 – 12 MPa
3	Drying	Temperature range	80 – 100 °C
4	Heat treatment	Temperature range	450 – 500 °C
		Heating rate	2 – 15 °C min^{-1}
		holding time	≥ 2 h
5	Mother liquor recovery and waste treatment	Temperature range	< 40 °C
		Recycling pH	4 – 5

Table S2. Structural parameters of XAYG1/250-UK

Structure	Parameter	Structure	Parameter	Structure	Parameter
Filter area	1 m^2	Number of plates	11 pieces	Foundation size	1100 mm
Flushing method	Side wash	Cylinder	100	Main beam form	Round steel
Pressing pressure	12 MPa	Back pressure	30 MPa	Size of filter plate	250×250 mm
Effluent form	Undercurrent	Pulling plate mode	Manual hydraulic	Feed hole position	Angular advance
Anti corrosion form	Plastic	Material temperature	normal temperature	Filter cloth	0303 permeability 1-3
Filter plate form	Plastic	Handle bottom height	110 mm	Filter plate form	High pressure diaphragm
Feed pressure	≤8 kg	Tympanic pressure	≤12 kg	Thickness of filter plate	40/35 room 10

Table S3. Time required for vacuum filtration and membrane filter press

Solid-liquid separation and washing methods	Filtration and washing time	Moisture content	Drying time	Total time for solid-liquid separation, washing, and drying
Vacuum filtration	5 h	70%	11 h	16 h
Membrane filter press	0.5 h	60%	7 h	7.5 h

Table S4. Products and treatment methods of PbO/RHAC preparation process

product	Main ingredients	Generated quantity	Treatment measures
Heat treatment gas products	H_2O	–200 g	Alkali absorption
	CO_2	–360 g	
Heat treated solid products	PbO, Pb, and amorphous carbon	–950 g	Load
Mother liquor	CH_3COONa、$(CH_3COO)_2Pb$、CH_3COOH	–590 L	Recycling

Table S5. Component quality of filtrate

Filtrate ion	Theoretical content (g)	Actual content (g)	Actual content / Theoretical content
Acetate ion	1057.90	1046.94	98.96%
Citrate ion	845.88	0.00	0.00%
Sodium ion	206.32	132.23	64.01%
Lead ions	927.36	15.13	1.63%

Table S6. Lead oxide and lead content in PbO/RHAC-T-t-r (determined by chemical titration)

Sample	Titration volume of PbO (mL)	Titration volume of Pb (mL)	PbO content (mg) and percentage (%)	Pb content (mg) and percentage (%)
PbO/RHAC-400-2-2	17.6	0.1	196.2 (19.6%)	1.0 (0.1%)
PbO/RHAC-450-2-2	17.2	0.5	191.8 (19.2%)	5.2 (0.5%)
PbO/RHAC-550-2-2	16.6	1.2	185.1 (18.5%)	12.4 (1.2%)
PbO/RHAC-450-2-15	17.4	0.3	194.0 (19.4%)	3.1 (0.3%)

Table S7. Tafel slope of different additives

No.	Composites	Tafel slope	Enhancement ratio	Reference
1	Pb@C-0.1	312 mV dec^{-1}	61.65%	[1]
2	HTT2000	187 mV dec^{-1}	92.78%	[2]
3	PbSAs@rGO	378 mV dec^{-1}	68.75%	[3]
4	**PbO/RHAC-450-2-2**	**408 mV dec^{-1}**	**124.59%**	**This work**

Table S8. Discharge capacity of 2 V/2 Ah battery at different rates

Battery	C_{10} (mAh)	C_3 (mAh)	C_1 (mAh)
Blank	2268.5	1882.1	1457.9
RHAC	2319.8	1941.6	1525.8
PbO/RHAC	2408.7	2086.7	1630.6

Table S9. Performance comparison of deep-cycle life

No.	Sample	Profiles of operation	Cycling life	Capacity retention rate	Reference
1	FLG	3.5 C 100% DoD	120	Not reported	[4]
2	AGM VRLA batteries	1 C 100% DoD	200	80%	[5]
3	SEPC-PbO	0.5 C 100% DoD	400	84%	[6]
4	Industrial LCB	0.1 C 70% DoD	480	80%	[7]
5	CB3	0.5 C 100% DoD	430	80%	[8]
6	Graphene	0.5 C 100% DoD	380	80%	[9]
7	**PbO/RHAC**	**0.5 C 100% DoD**	**593**	**80%**	**This work**

Table S10. Material balance for large scale preparation of PbO/RHAC

Process Unit	Input name	Input mass	Output name	Output mass
Complexation precipitation reaction	RHAC	4 kg	Lead citrate/RHAC/Sodium acetate/Acetic acid/Water	57.62 kg
	Sodium acetate	1.22 kg		
	citric acid	0.94 kg		
	Lead acetate	1.46 kg		
	pure water	50 L		
Solid-liquid separation and washing	Lead citrate/RHAC/Sodium acetate/Acetic acid/Water solid-liquid mixture	57.62 kg	Lead citrate/RHAC/water	13.63 kg
	Washing water	546 L	Lead acetate/sodium acetate/acetic acid/water mixture	589.99 kg
Drying	Lead citrate/RHAC/water	13.63 kg	Lead Citrate/RHAC	5.45 kg
Heat treatment	Lead Citrate/RHAC	5.45 kg	PbO/RHAC	4.95 kg
Mother liquor recovery and waste treatment	Residual lead acetate	23.75 g	Supplement lead acetate	1.44 kg

Table S11. Yield and Recovery rate in the large-scale preparation process of PbO/RHAC

Materials	Yield (kg)	Recovery rateγ (%)	Overall recovery rateγ (%)
Theoretical yield of lead citrate	1.57	92.4	96.2
Actual yield of lead citrate	1.45		
Theoretical yield of lead citrate/RHAC precursor	5.57	97.8	
Actual yield of lead citrate/RHAC precursor	5.45		
Theoretical yield of PbO/RHAC	5.03	98.4	
Actual yield of PbO/RHAC	4.95		

Table S12. Economic evaluation of green large-scale preparation process of PbO/RHAC

Materials	Unit price	Consume [a] or produce [b]	Cost [a] or price [b] (¥)
Rice husk activated carbon [a]	100.00 ¥ kg^{-1}	-4.00 kg	-400.00
Sodium acetate [a]	6.8 ¥ kg^{-1}	-1.22 kg	-8.30
Citric acid [a]	27.00 ¥ kg^{-1}	-0.94 kg	-25.38
Lead acetate [a]	34.00 ¥ kg^{-1}	-1.43 kg	-48.62
Water [a]	2.00 ¥ t^{-1}	-0.59 t	-1.18
Nitrogen [a]	0.04 ¥ L^{-1}	-1440.00 L	-57.60
Electricity [a]	0.45 ¥ kWh^{-1}	-80.00 kWh	-36.00
PbO/RHAC [b]	180 ¥ kg^{-1}	+4.95	+891.00
Total cost	--	--	-577.08
Unit cost			116.58
Total revenue	--	--	891.00
Gross profit	--	--	313.92
Unit gross profit			63.42
Gross margin	--	--	35.23%

Gross margin = (total revenue - total cost) / total revenue.

a and b represent raw materials and products, respectively, denoted by negative and positive values.

Text S1: The electrochemical performance of PbO/RHAC was evaluated using graphite-based membrane electrodes. Test materials, acetylene black, and polytetrafluoroethylene were uniformly dispersed in 20 mL of ethanol at a mass ratio of 85:10:5. The mixture was heated and stirred at 90 °C to form a homogeneous blend, which was then rolled into a uniform carbon film. After drying the carbon film at 80 °C for 12 h, it was cut into carbon discs measuring 10.00 × 10.00 mm^2 (5.00 ± 0.1 mg). Finally, the carbon discs were laminated onto graphite sheets under 5 MPa pressure. The exposed graphite areas around the periphery were sealed with epoxy resin and air-dried to produce graphite-based membrane electrodes [10].

Performance testing of PbO/RHAC as anode additives was conducted in 2 V/2 Ah test batteries. The anodes were prepared using a typical paste method. Short polymer fibers, $BaSO_4$ particles, sodium lignosulfonate, acetylene black, and humic acid were uniformly mixed in a proportion of 0.13 wt.%, 0.80 wt.%, 0.20 wt.%, 0.20 wt.%, and 0.20 wt.%, respectively, relative to the mass of lead oxide powder. The mixture was further blended with 11.50 wt.% pure water and 8.80 wt.% sulfuric acid solution (1.41 g cm^{-3}) to form a paste. This paste was uniformly coated onto Pb-Sn-Ca alloy grids. The coated negative plates were flattened using a roller and then immersed in sulfuric acid (1.14 g cm^{-3}) for 3 seconds. Subsequently, a curing and drying process was conducted in four stages: 50 °C, 98% humidity, cured for 24 h; 55 °C, 80% humidity, cured for 15 h; 60 °C, 30% humidity, cured for 3 h; 70 °C, 10% humidity, cured for 3 h. The resulting anode plate was designated as Blank. The LCB anode paste was prepared using a similar process, but with the additional incorporation of 1.00 wt.% RHAC base material.

The cured positive and negative plates are assembled with the AGM separator separating the electrodes. The active material masses for the positive and negative electrodes are 22.00±0.1 g and 16.0±0.1 g, respectively. The 2 V/2 Ah test battery consists of two commercial positive plates and one handcrafted negative plate. The battery undergoes initialization after soaking in sulfuric acid solution (1.24 g cm^{-3}) for 2 h. The initialization steps are as follows: first, charge at 0.0667 C_2 for 1 h, then at 0.25 C_2 for 16 h, followed by charging at 0.1333 C_2 for 2 h. Subsequently, discharge at

0.4167 C_2 until reaching 1.8 V. The second stage involved repeating the above charge-discharge cycle three times, followed by final charging at 0.125 C_2 for 8 h and 0.0417 C_2 for 2 h [11]. A sulfuric acid solution with a concentration of 5 mol L^{-1} was used as the electrolyte for the cell.

Text S2:

Electrochemical testing employed a three-electrode system comprising a working electrode (WE) made of a graphite-based membrane electrode, a graphite plate as the counter electrode (CE), and a mercurous sulfate Hg/Hg_2SO_4 reference electrode (RE). The electrolyte consisted of an aqueous H_2SO_4 solution (1.28 g cm^{-3}). Testing was conducted using a Princeton Multichannel Electrochemical Testing System (PMC-1000). Cyclic voltammetry (CV) and linear sweep voltammetry (LSV) were performed over a potential range of -0.40 V to -1.40 V, with scan rates of 10 mV s^{-1}, and 1 mV s^{-1}, respectively. Specific capacitance values were obtained according to Equation 1 below.

$$C = \frac{1}{2A\upsilon\Delta V}\int_{v_1}^{v_2} I(V)\,dV \tag{1}$$

Here, C represents the specific capacitance (mF cm^{-2}), A is the area of the working electrode (cm^{-2}), υ represents the scan rate (V s^{-1}), ΔV is the potential window width (V), and $\int_{v_1}^{v_2} I(V)\,dV$ represents the integrated area of the CV curve. Electrochemical impedance spectroscopy (EIS) was performed at open circuit potential, with a voltage amplitude of 10 mV, and a frequency range of 100 kHz to 0.01 Hz. All EIS test data were fitted to specific values using ZSimpWin software based on the equivalent circuit diagram.

Electrochemical double-layer capacitance (C_{dl}) testing is conducted via cyclic voltammetry within the non-faradaic region where no redox reactions occur. Centering on the open-circuit voltage (OCV) with a ±50 mV testing range, measurements were conducted at scan rates of 60 mV s^{-1}, 80 mV s^{-1}, 100 mV s^{-1}, 120 mV s^{-1}, and 140 mV s^{-1}. The C_{dl} values were obtained using the formula in Equation 2 below.

$$C_{dl} = I_C/\upsilon, \tag{2}$$

In the equation, I_C represents the double-layer current density, also known as the non-faradaic current, whose value is half the difference between the charging and

discharging current densities, i.e., ($\Delta J=J_a-J_c$)/2. υ denotes the scan rate. Plotting I_C versus υ yields a slope corresponding to the C_{dl} value.

In a three-electrode system, the electrochemistry of the negative plate generally uses a small negative plate (0.6 g, 8 mm × 15 mm × 1.5 mm) after formation as the working electrode, a formed commercial positive plate as the counter electrode (40.00 mm × 68.00 mm × 2.20 mm), mercurous sulfate (Hg/Hg_2SO_4) as the reference electrode, and H_2SO_4 (1.28 g cm^{-3}) as the electrolyte. Before electrochemical tests, the working electrode underwent 30 CV cycles at a scan rate of 50 mV to complete the activation process. The CV test potential range was: -1.40 V to -0.40 V, with a scan rate of 5 mV s^{-1}. The LSV test potential range was -0.60 V to -1.60 V, with a scan rate of 1 mV s^{-1}. EIS tests were performed at open circuit potential and -1.30 V potential, respectively, with a voltage amplitude of 10 mV and a frequency range of 100 kHz to 0.01 Hz.

All battery charge and discharge performances were tested using a battery tester (BTS 5V/6A, Shenzhen Neware Technology Co., Ltd., China). Unless otherwise specified, all test charging procedures employed constant current and constant voltage (2.40 V, 0.2 C_{10}) for 7 h or until the cutoff current reached 0.01 C_{10}. During rate capacity testing, fully charged batteries were discharged at currents of 0.1 C_{10}, 1/3 C_3, and 1 C_1 to voltages of 1.80 V, 1.70 V, and 1.60 V, respectively, with discharge capacity recorded. In the charge acceptance test, fully charged batteries were discharged at a current of I_{10} for 5 h in a constant-temperature water bath maintained at 25 °C. Immediately after discharge completion, the batteries were placed in a 0 °C low-temperature chamber for 20 h. Subsequently, the batteries underwent constant-voltage charging at 2.40 V ± 0.10 V, with the charging current I_{ca} recorded at the 10-minute mark post-charging initiation. The ratio of I_{ca} to I_{10} serves as an indicator of charge acceptance capacity [12]. In the HRPSoC cycle test, fully charged batteries were discharged to 50% SoC at a 1 C_1 current. This is followed by a 2 C_1 high-rate shallow cycle charge-discharge. The cycle process is as follows: 60 s of 2 C_1 charging and 60 s of 2 C_1 discharging; a 10 s rest period after each charge and discharge cycle until the discharge voltage reaches 1.75 V. Then, high-rate shallow cycling charge and discharge

at 2 C_1 was performed. The cycling process was as follows: 2 C_1 charge and discharge for 60 s each; after each charge and discharge, a 10 s rest period was applied until the discharge voltage reached 1.75 V. These three consecutive HRPSoC test blocks were each preceded by a full recharge of the battery. In the 0.5 C 100% DoD cycle test, the battery is charged for 7 hours by constant current and constant voltage (2.40 V, 0.2 C_2) or the cut-off current is 0.01 C_2. Then it is discharged to 1.75 V with 0.5 C_2, and each charge and discharge above is a cycle. When the discharge time for three consecutive times is less than 96 min (less than 80% of the discharge time), the battery is judged to be invalid, and the cycle life test is completed.

Text S3:

DFT calculation in this work was executed via the Vienna ab initio simulation package (VASP) software. For the exchange-correlation energy, the Perdew-Burke-Ernzerhof (PBE) form of the generalized gradient approximation (GGA) was adopted. The partial occupancies of wave functions were determined by the Gaussian smearing method, with a smearing width of 0.05 eV applied to smooth energy levels. In addition, the DFT-D3 correction term was used to accurately handle van der Waals forces. To ensure calculation accuracy, the plane-wave cutoff energy was set to 400 eV. The SCF convergence criterion was 1×10^{-7} eV. All systems were optimized until the maximum force on any single atom was below the convergence criterion of 0.02 eV/Å. For Brillouin zone sampling, k-point calculations were performed only at the Γ-point, to simplify calculations while maintaining sufficient accuracy. Considering computational efficiency and practical context, we set a 15 Å vacuum layer in the model to isolate adjacent periodic images. Solvation effects were ignored in the calculations of this study. The adsorption energy (E_{ads}) of PbO was determined by the given equation: $E_{ads} = E_{total} - E_{fragment} - E_{PbO}$, where E_{total}, $E_{fragment}$, and E_{PbO} represent the total energy with PbO adsorbed, the total energy without PbO adsorbed, and the energy of PbO, respectively.

References

1. P. He, Y. Yang, H. Huang, J. Huang, H. Wang, Y. He and Z. Guo, *Journal of Energy Chemistry*, 2024, **97**, 486-497.
2. J.-H. Wee, K. Nomura, H. Nishihara, D.-W. Kim, S. Hong, G. B. Choi, S. Y. Yeo, J. H. Kim, H.-Y. Jung and Y. A. Kim, *Carbon*, 2021, **185**, 419-427.
3. D. Tao, X. Liu, Z. Li, H. Yang, J. Wang and Q. Zhang, *Chemical Engineering Journal*, 2023, **461**, 141992.
4. S.-H. Chang, K.-C. Kung, W.-C. Huang and W.-R. Liu, *Thin Solid Films*, 2022, **753**, 139273.
5. T. Tantichanakul, O. Chailapakul and N. Tantavichet, *Journal of Power Sources*, 2011, **196**, 8764-8772.
6. Y. T. Hu, J. C. Li, A. Ali and P. K. Shen, *Journal of Energy Storage*, 2021, **41**, 102785.
7. , !!! INVALID CITATION !!! .
8. H.-Y. Hu, N. Xie, C. Wang, F. Wu, M. Pan, H.-F. Li, P. Wu, X.-D. Wang, Z. Zeng, S. Deng, M. H. Wu, K. Vinodgopal and G.-P. Dai, *Journal*, 2019, **9**.
9. H.-Y. Hu, N. Xie, C. Wang, L.-Y. Wang, R. M. Privette, H.-F. Li, M. Pan, F. Wu, X.-L. Yan, B.-B. Jiang, M. H. Wu, K. Vinodgopal and G.-P. Dai, *ACS Omega*, 2018, **3**, 7096-7105.
10. L. Wang, H. Zhang, G. Cao, W. Zhang, H. Zhao and Y. Yang, *Electrochimica Acta*, 2015, **186**, 654-663.
11. J. Yin, N. Lin, W. Zhang, Z. Lin, Z. Zhang, Y. Wang, J. Shi, J. Bao and H. Lin, *Journal of Energy Chemistry*, 2018, **27**, 1674-1683.
12. A. A. Moustafa, A. M. Ashmawy, I. M. Ghayad, A. A. El-Zomrawy and S. M. Abdelbasir, *Journal of Energy Storage*, 2022, **56**, 105932.